

RESEARCH

Open Access



# Interaction studies unveil potential binding sites on bovine serum albumin for gut metabolite trimethylamine n-oxide (TMAO)

Awadhesh Kumar Verma<sup>1,3</sup>, Payal Gulati<sup>2</sup>, GBVS Lakshmi<sup>1</sup>, Anand Mohan<sup>3</sup>, Neeta Raj Sharma<sup>3</sup>, Pratima R. Solanki<sup>1</sup> and Anil Kumar<sup>2\*</sup>

## Abstract

Trimethylamine-N-oxide (TMAO) is gut microbiota-derived metabolite, plays a critical role in human health and diseases such as metabolic, cardiovascular, colorectal cancer and, neurological disorders. Binding interactions between TMAO and serum albumins are crucial to understand the impact of TMAO on disease mechanisms. However, detailed insights into the interaction mechanisms, preferred binding locations, and conformational changes in BSA upon binding TMAO are still unclear. TMAO interacts with serum albumin in human body and thus, a model study of interaction for TMAO-BSA conjugate is presented in support of it. Decrease in absorbance intensity of protein upon interaction with metabolites reveals conjugate formation, while fluorescence spectroscopy indicate static quenching. Contact angle measurements further reveal the hydrophilic nature of the TMAO-BSA complex, while CD and FTIR support conformational changes in BSA upon binding but structure remain intact. Computational studies, such as molecular docking, molecular dynamics simulation and, MM/GBSA, confirm a stable complex with a binding energy of  $-3.6$  kcal/mol. These findings provide a foundation for understanding the pharmacodynamics and pharmacokinetics of TMAO and may aid in developing strategies for treating diseases, such as chronic kidney disease and neurological disorder where TMAO-serum albumins interaction are implicated.

**Keywords** TMAO, Bovine serum albumin (BSA), In silico, DFT, Docking, Spectroscopy, Molecular dynamics simulation, Mmgbsa

## Introduction

The human gut is the primary source of Trimethylamine-N-oxide (TMAO). There, the gut microbiota breaks down food components into TMA, which is taken into the bloodstream via the intestinal mucosa. Hepatic flavin

monooxygenases in the liver subsequently convert TMA into TMAO [1, 2]. As per recent research reports, circulating TMAO is becoming known to be associated with an increasing variety of other chronic conditions, such as cancer, type 2 diabetes mellitus (T2DM), and renal disease as mentioned in Fig. 1. Here is the specific mechanism. TMAO (trimethylamine-N-oxide) has been linked to cancer through mechanisms that activate pro-inflammatory pathways (e.g., NF- $\kappa$ B, MAPK), increase oxidative stress by enhancing reactive oxygen species (ROS), and dysregulate cellular metabolism, particularly lipid and cholesterol processing. These combined effects foster a microenvironment conducive to tumor development, positioning TMAO as a promising target for

\*Correspondence:

Anil Kumar  
anilk@nii.ac.in

<sup>1</sup> Special Centre for Nanoscience, Jawaharlal Nehru University, New Delhi 110067, India

<sup>2</sup> Gene Regulation Laboratory, National Institute of Immunology, Aruna Asaf Ali Marg, New Delhi 110067, India

<sup>3</sup> School of Bioengineering and Biosciences, Lovely Professional University, Phagwara 144411, Punjab, India



© The Author(s) 2025. **Open Access** This article is licensed under a Creative Commons Attribution-NonCommercial-NoDerivatives 4.0 International License, which permits any non-commercial use, sharing, distribution and reproduction in any medium or format, as long as you give appropriate credit to the original author(s) and the source, provide a link to the Creative Commons licence, and indicate if you modified the licensed material. You do not have permission under this licence to share adapted material derived from this article or parts of it. The images or other third party material in this article are included in the article's Creative Commons licence, unless indicated otherwise in a credit line to the material. If material is not included in the article's Creative Commons licence and your intended use is not permitted by statutory regulation or exceeds the permitted use, you will need to obtain permission directly from the copyright holder. To view a copy of this licence, visit <http://creativecommons.org/licenses/by-nc-nd/4.0/>.

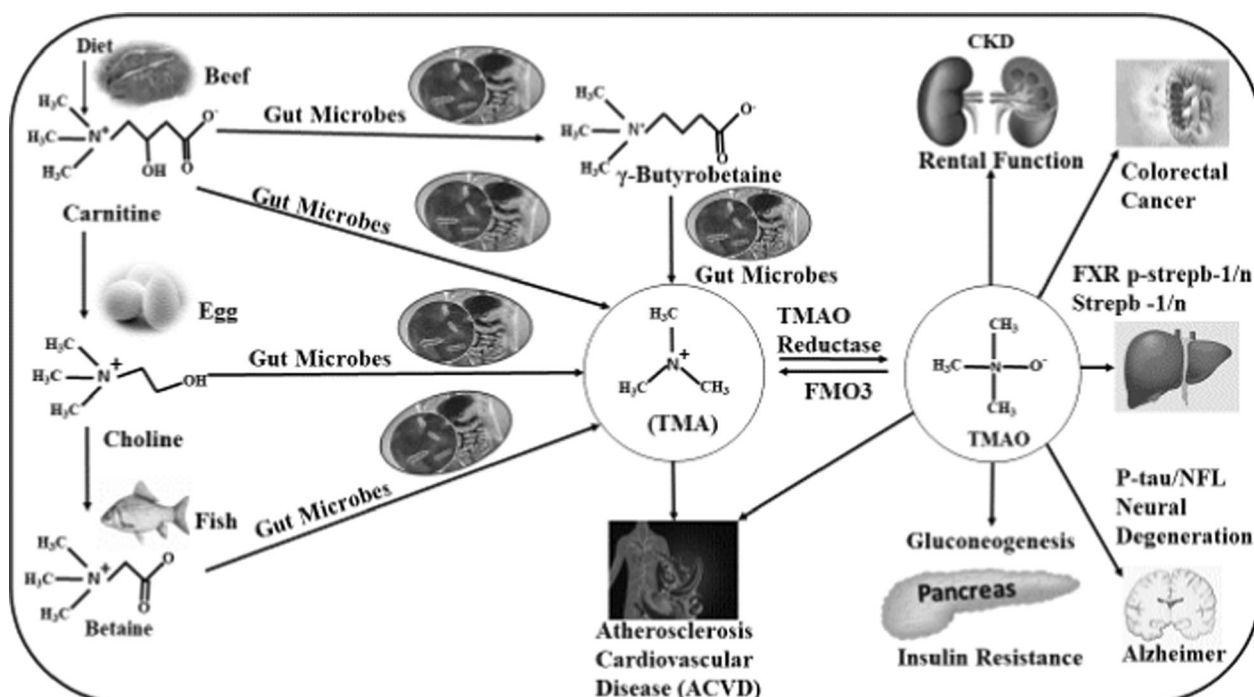


**Fig. 1** Formation of TMAO from various precursor obtained from ingested foods and its implications in different diseases

cancer prevention strategies [3]. The role of TMAO in T2DM via gut microbiota alterations, inflammation, and cardiovascular risk, all contributing to insulin resistance and metabolic imbalance. TMAO has been shown to impair insulin signaling pathways, particularly by activating inflammatory mediators (e.g., TNF- $\alpha$ , IL-6) that promote insulin resistance in hepatic and peripheral tissues. TMAO levels are influenced by gut microbiota composition, where dysbiosis promotes increased TMAO synthesis, which disrupts glucose metabolism and exacerbates metabolic syndrome. Also, TMAO has been found to enhance oxidative stress and lipid accumulation, particularly in the liver, contributing to beta-cell dysfunction and progressive glucose intolerance. TMAO promotes endothelial dysfunction and triggers inflammation by activating pro-inflammatory cytokines, exacerbating kidney tissue damage in chronic kidney disease (CKD) patients. Elevated TMAO levels are associated with increased phosphate levels, which is common in renal disease, further impairing kidney function and contributing to CKD progression [4]. In CKD, gut dysbiosis significantly contributes to TMAO buildup, which disrupts kidney function by intensifying uremic toxin levels and inflammatory responses [5]. The biological effects of TMAO vary among several animals and tissue types. Water-stressed organisms and tissues use TMAO as an organic osmolyte to preserve cell volume. The capacity of TMAO to modify the structure and activity of a

broad class of physiologically significant molecules is one of its roles. TMAO plays a significant stabilizing role in nucleic acid and the folded state of proteins. TMAO is a protein-stabilizing osmolyte, which enhances stability by counteracting denaturants and preserving protein folding. TMAO stabilizes proteins primarily by enhancing hydrogen bonding and reducing the solvent-accessible surface area around the protein backbone, which supports its native folding structure even under stress conditions like high urea concentrations or temperature. By interacting preferentially with water, TMAO promotes protein compactness, decreasing denaturation and aggregation. In the protein backbone, TMAO contributes to the maintenance of functional conformations, enhancing stability without interfering directly with the protein's active sites, thus preserving activity [6, 7]. Studies on the thermodynamic effects of TMAO on proteins have demonstrated that TMAO inhibits denaturation of proteins and mitigates the effects of heat and pressure [8]. TMAO indirectly stabilizes carbohydrate molecules by maintaining the active conformation of glycoside hydrolase enzymes essential for carbohydrate metabolism. It strengthens hydrogen bonds and reduces enzyme flexibility under stress, ensuring efficient carbohydrate breakdown. Additionally, TMAO forms a favorable hydration shell around these enzymes, supporting catalytic efficiency across various cellular environment conditions [9]. TMAO stabilizes lipid bilayers by promoting tighter

packing of lipid molecules, enhancing membrane integrity and reducing fluidity. This organization supports the formation of ordered lipid domains, which strengthens the cell membrane against stress [10]. TMAO stabilizes DNA and RNA by promoting helical structure integrity, especially under destabilizing conditions like high temperature or chemical stress. It achieves this by reinforcing hydrogen bonds between nucleotide bases and creating a hydration shell around the nucleic acids, which reduces unfolding. This protective environment helps preserve the functional configurations of DNA and RNA necessary for cellular processes [11]. The accumulation of TMAO by the kidneys of mammals is a response to the destabilizing effects of urea (as well as inorganic ions) on macromolecular structures, such as proteins and nucleic acids, and to the inhibition of urea on activities, including ligand binding [12].

The main extracellular protein of the circulatory system, serum albumin, makes up roughly 60% of all plasma proteins [13]. It transports various medications, fatty acids, thyroid hormones, and steroids and gut microbiota derived metabolites such as TMAO, TMA, indoxyl sulfate etc. [14]. Because it is more readily available and less expensive, BSA is frequently used in place of human serum albumin (HSA) in laboratory investigations. Because of their 88% and 76% closeness in amino acid sequences, BSA and HSA have comparable binding capacities [15]. BSA shows greater stability under diverse solvent conditions compared to HSA, which enhances its consistency in studies involving TMAO interactions. BSA's structural adaptations to osmolytes, such as TMAO, provide clearer insights into protein–ligand binding dynamics at high pressures, making it a robust model [16]. BSA's higher amino acid flexibility than HSA enhances its responsiveness to osmolytes like TMAO, ideal for mimicking cellular osmotic stress [17]. HSA, which can indeed affect binding interactions and overall protein behavior. While BSA serves as a practical model, we recognize that these differences may limit direct extrapolation to human contexts. While BSA and HSA share significant structural and functional characteristics, subtle differences, such as variations in amino acid sequences and binding sites, can affect how each protein interacts with stabilizing osmolytes like TMAO [18]. Including a comparison of these structures would help the reader assess whether TMAO's stabilizing effect on BSA is likely to be mirrored in HSA. This is particularly important as even small differences in surface residues or binding pocket configurations can impact ligand binding and protein stability. BSA often serves as a model for studying protein behavior due to its structural similarity to HSA. However, drawing more explicit connections to HSA would enhance the biological relevance of

the findings for human physiology. For instance, TMAO's protective effects could have implications for HSA stability and function in human blood, potentially impacting drug binding, transport functions, or responses to osmotic stress. Such insights could lead to a better understanding of HSA's stability in therapeutic settings or under pathological conditions. Since elevated levels of TMAO have been linked to human disease states (e.g., cardiovascular disease), an expanded discussion on how TMAO might interact with HSA in the human circulatory system would be relevant. Exploring how TMAO impacts HSA stability and function in humans could help in understanding its role in health and disease, especially given the differences between HSA and BSA in ligand-binding properties and susceptibility to structural change under physiological stresses [19]. BSA and HSA could clarify the translational potential of these findings. This could include discussing how differences in albumin structure and function between species may affect TMAO's stabilizing impact, thereby shedding light on the physiological relevance of TMAO in human health and disease contexts. Moreover, BSA provides a model study of interaction with small metabolites. Future studies could include HSA-specific analyses to strengthen relevance to human health, addressing any concerns of applicability. Moreover, we have conducted the experiment with HSA also with same small metabolite and results were similar in both experimental as well as computational analysis and the paper was communicated. Numerous studies have been conducted to examine the binding between gut microbial metabolites and natural chemicals with serum albumin [20–24]. Because serum albumin is a drug's transport carrier and has a major impact on its bioavailability, research on the relationship between albumin and TMAO is crucial. The capacity of these gut metabolites to bind determines how successful they are as pharmacological agents [25, 26]. Although TMAO has been extensively documented for its actions and implication in human health and diseases, no clear scientific data about its interaction with serum albumin is available. Kaempferol's dual emission in a serum albumin environment underscores its utility as a versatile fluorescent probe for protein–ligand studies. The strong binding interactions observed through spectroscopic and molecular docking analyses further highlight its potential for probing protein environments and interactions.[27]. Hydroxytyrosol (HT) interacts strongly with BSA, primarily through hydrophobic forces, as shown by fluorescence spectroscopy and molecular docking, suggesting a stable binding mechanism [28]. Antimony potassium tartrate and potassium pyroantimonate form a modestly bound 1:1 complex with BSA, as shown by fluorescence quenching and UV–vis spectra, highlighting distinct

binding interactions based on antimony's chemical form [29]. Luteolin binds to hen egg white lysozyme (HEWL) with moderate affinity through hydrophobic interactions, primarily at Trp62, involving a static quenching mechanism that stabilizes the protein–ligand complex [30]. Epigallocatechin gallate (EGCG) binds moderately to bovine hemoglobin (BHB) near  $\beta$ 2-Trp37, primarily stabilized by hydrophobic forces, inducing structural changes that enhance protein stability and inhibit glycation [31]. 4-Ethyl phenyl sulfate (4-EPS) binds to BSA with moderate affinity, inducing structural changes and fluorescence quenching, suggesting a stable complex that could inform therapeutic strategies for toxin clearance [32]. Highlighting aptamers as molecular tools that offer high selectivity and stability in binding interactions with target proteins, making them effective in targeted drug delivery and diagnostics [33]. The studies collectively illustrate that compounds such as hydroxytyrosol, antimony complexes, and 4-ethyl phenyl sulfate demonstrate specific binding interactions with BSA, predominantly via hydrophobic forces or moderate binding affinities. These interactions not only stabilize BSA but also showcase the potential of BSA–ligand complexes in exploring therapeutic applications, protein stability, and toxin clearance strategies.

In context to the physiological conditions, studying the TMAO–BSA interaction sheds light on how TMAO influences BSA's stability, transport functions, and structural integrity within the circulatory system. This has important implications for maintaining homeostasis, protein function, and resilience under the conditions encountered in the human body, including variations in pH, temperature, and osmotic pressure. BSA, like its human counterpart HSA, circulates in the blood, exposed to fluctuations in temperature, pH, and osmotic pressure. TMAO stabilizes BSA's  $\alpha$ -helical structure, helping it resist denaturation from these physiological stressors. This effect supports the maintenance of BSA's structural integrity, which is crucial for its role as a transporter in the bloodstream under varying physical and metabolic conditions [34]. BSA is essential for maintaining oncotic (colloid osmotic) pressure, which helps regulate fluid balance between blood vessels and tissues. By stabilizing BSA, TMAO indirectly contributes to sustaining oncotic pressure in blood plasma, which prevents excessive fluid leakage into tissues. This is vital for blood pressure maintenance, vascular health, and preventing edema, especially under conditions like dehydration or altered osmotic gradients [35]. TMAO's stabilizing effect on BSA helps preventing aggregation by preserving its native structure, which is beneficial in maintaining blood flow and preventing protein-related pathologies under physiological stress conditions. Also, TMAO exemplifies how nature uses the solute effect as a simple chemical

strategy to cope with hydrodynamic pressure or urea stress to maintain proteostasis [36]. BSA's function as a transporter depends on maintaining its binding sites for hormones, fatty acids, metabolites, and drugs. TMAO helps stabilize these binding sites, ensuring that BSA's transport functions are preserved despite physiological changes. In pathological conditions like oxidative stress, inflammation, or cardiovascular disease, proteins in blood circulation are more vulnerable to destabilization. Elevated TMAO levels could help stabilize BSA under these conditions, reducing the risk of structural alterations and maintaining BSA's function in transport and osmotic regulation. This protective role is important for understanding TMAO's complex impact on health, as it may support protein stability under stress while also having context-dependent effects in disease [19].

The interaction of TMAO and proteins such as BSA can involve physical binding, changes in protein conformation, and potential functional effects. As the mechanism behind specific binding of TMAO with BSA and the effect of TMAO on protein conformation are not clear, hence in the present study, efforts have been made to study these aspects in detail. It is evident that conformational change in serum albumin is prompted by interaction with metabolites such as TMAO, drugs molecules and dyes having lower molecular weight, that significantly alter the albumin secondary and tertiary structure [37]. Therefore, binding of gut metabolite TMAO with serum albumin is very important in the field of biomedical research. This study investigated the binding between BSA with TMAO. The binding relationship was investigated using multi-spectroscopic (UV–vis absorption, CD, fluorescence, FT-IR) and contact angle methods. In addition, molecular docking studies were performed to better visualize the binding mode with BSA. Study parameters included TMAO binding energies with BSA, complex formation, and binding site involvement.

## Experimental section

### Reagents and buffer

BSA in lyophilized form (CAS Number: 9048–46–8, Product Number: SRE0096), and Trimethylamine N-Oxide (TMAO) (CAS Number: 1184–78–7 product number 317594) with high purity were procured from Sigma Aldrich. Dialysis membrane (Snake Skin™ Dialysis Tubing, 10K MWCO, 16 mm) (product Number: 88243) was procured from Thermo Scientific. Glacial acetic acid (C.A.S Number 64–19–7, Product code: 569) was procured from TM Media. Sodium acetate (CAS 127–09–3, 106268) was procured from Merck. Methanol (CAS: 67–56–1, 96446), from SRL Ranbaxy and ethanol (CAS #: 64–17–5 EC Number: 200–578–6) were procured from Merk. 0.2-micron filter was procured from MDI

(Catalog No.NC1645612) and 2 ml syringe was procured from HMD. MilliQ (18.2 M $\Omega$  cm @ 25 °C) from the Millipore water purification system was used for preparation of all the solutions. Acetate buffer at pH 4.3 was used for TMAO-BSA conjugate preparation. To keep the protein active and stable, the pH of the experimental operating buffer must be within 1.0 pH point of their pI. Moreover, in bioconjugation, the adsorption plays an important role, which is higher near the pI of the protein [38, 39]. Therefore, we have conducted our experiments at pH 4.3 which is within 1.0 pH unit of pI of BSA i.e. 4.7–5.2. The hydrophobic force is dominant at this pH 4.3 rather than hydrophilic. This can be correlated with the contact angle obtained as the BSA concentration was fixed and metabolite concentration was increased therefore the hydrophilicity was found to be increased as the contact angle were decreasing. The same has been incorporated in the manuscript at Sect. “Reagents and Buffer”.

#### Instrumentation

##### UV-vis spectroscopy

The UV-vis absorption spectra of BSA were taken in the absence and presence of TMAO using UV-2600, UV-VIS Spectro-photometer SHIMADZU (Shimadzu Corporation in Japan), through 1.0 cm quartz cells keeping slit width 5 nm and 600 nm/minute scan speed. The spectra were recorded in wavelength range between 200 and 600 nm.

##### Fluorescence studies

Fluorescence was measured with the help of Fluorescence spectrophotometer (Cary Eclipse, Model G9800A, Agilent Technology,) with fixed excitation as well as emission slit width (5 nm) and 600 nm/minute scan speed. A quartz cuvette (3.5 ml) with path length 10 mm was used.

##### FTIR

To determine the functional groups changes, residing on the surfaces of bio-conjugates; FTIR spectrophotometer were used in ATR mode (PerkinElmer Spectrum 1). The spectra were obtained in between range of 4000–400 wavenumber, with scan speed of 32.

##### CD Spectroscopy

CD spectroscopic study was performed to monitor the effect of TMAO on secondary and tertiary structure of BSA in acetate buffer solution (pH 4.3). CD spectra were obtained in the UV region using JASCO-1500 CD spectropolarimeter associated with a Peltier temperature controller (PTC-517). Molecular ellipticity was recorded in the far-UV range from 190 to 250 nm using a cell (path length 1 mm) at room temperature (25 °C), 1 nm

bandwidth. The average of three measurements were displayed as final spectra with mean time 1 nm/sec.

##### Contact angle

The contact angle measurement was done using drop shape analyzer (KRUSS, Germany) to check the hydrophobicity/hydrophilicity of the TMAO-BSA conjugate on ELISA plate.

##### Conjugate preparation

TMAO (in acetate buffer, PH=4.3) was conjugated with BSA (acetate buffer, pH=4.3) in different molar ratios including 1:1, 1:5, 1:10, 1:25, 1:50, 1:75, 1:100. A 3.5 mM of TMAO was mixed with 15  $\mu$ M of BSA and allowed to react for 2 h at room temperature and for 72 h at 4 °C. At the end of the reaction, dialysis was performed for 72 h with change of acetate buffer (pH=4.3) after every 12 h.

##### Computational details

##### Molecular modeling and optimization of TMAO using DFT

We have theoretically modeled 3D structure of gut metabolite TMAO using Marvin sketch software. Every time 2D and 3D cleaning was performed and 3D structural confirmation of the molecule was checked by visualizing them in Marvin view. Further, we calculated each and every parameter like atomic coordinates (XYZ), bond length, and bond angle using ChemBioDraw Ultra software and optimized the structure up to transition state followed by energy minimization using MM2 via Chemdraw and Chem3DPro. The final optimization was done via DFT approach with Gaussian 09 software with standard basis set: 6-311G and RB3LYP functional. This optimized structure was further utilized for docking to monitor the interactions between TMAO and BSA molecule [40].

##### Preparation of receptor molecule

BSA structure (Source organism: *Bos Taurus*, resolution: 2.70 Å and having 583 amino acid residues) was retrieved from Protein Data Bank having RCSB PDB ID: 3V03 [41]. The structure was cleaned of crystallographic water molecules and other crystalizing agents. Polar hydrogens including Kollmann charges were added, also Gasteiger charges were computed. The atomic type was assigned AD4 type.

##### Molecular docking

Finally, rigid molecular docking was performed with the optimized TMAO molecule to find the binding affinity and binding energy of TMAO-BSA conjugate using Autodock 4.2 software tools. A genetic algorithm simulation program was used with a population size of 300 and 100 runs. The remaining parameters were kept as it is to their default

values. The output docked file was saved as Lamarckian GA. The top 10 confirmations of protein–ligand complex were saved on based on their negative binding energy ( $\Delta G$ ) and RMSD values. PyMol, VMD LigPlot<sup>+</sup>, and discovery studio softwares were taken into consideration to study the interaction and binding energy of TMAO-BSA conjugate [42].

### MD simulation and MM/GBSA

In our research to monitor the TMAO-BSA interaction, we have used the Schrodinger suite for MD Simulation. Molecular dynamics production was performed till 150 ns with NPT (normal pressure & temperature) conditions. To know the real-time interaction energy of the TMAO-BSA complex we performed the post facto free-energy component analysis using MM/GBSA [43]. OPLS\_2005 has been used for force field parameters. Here the binding energy of the receptor and ligand is calculated by the Prime Energy i.e. molecular mechanics and implicit solvent energy function (kcal/mol).

## Results and discussion

The interaction between metabolite (TMAO) and BSA is studied using the following spectroscopic techniques.

### UV–Visible spectroscopy and fluorescence study

UV–visible absorbance spectra of TMAO, BSA and TMAO-BSA (deducting TMAO absorbance spectrum in acetate buffer, pH 4.3 and the concentration of TMAO were taken as 2, 10, 20, 50, 100, 150 and 200  $\mu\text{M}$  respectively) solutions measured separately to ensure the mechanism of quenching.

Since the absorbance of BSA is significantly high in comparison to TMAO absorbance as observed in Fig. 2a, b. Therefore, due to interaction of metabolite with BSA causes a decrease in absorption values from 0.84 to 0.48 as seen in Fig. 2c. Further, as BSA absorption is high therefore on deducting the BSA absorbance from the TMAO-BSA conjugate gives negative values as seen in Fig. 2d. This is confirmed by Fig. 2e that on deducting the TMAO absorbance from the TMAO-BSA conjugate shows a significant decrease in absorbance value which confirms that interaction is taking place between TMAO and BSA.

Figure 3a shows that absorbance of BSA around 280 nm decreases with the stepwise addition of TMAO solution in different concentrations. This suggests that quenching in absorbance of BSA occurred mainly due to TMAO-BSA conjugate formation [44]. The absorbance around 280 nm is primarily due to the presence of aromatic amino acids like Trp, Tyr, and Phe in the protein structure. Aromatic amino acids like tryptophan

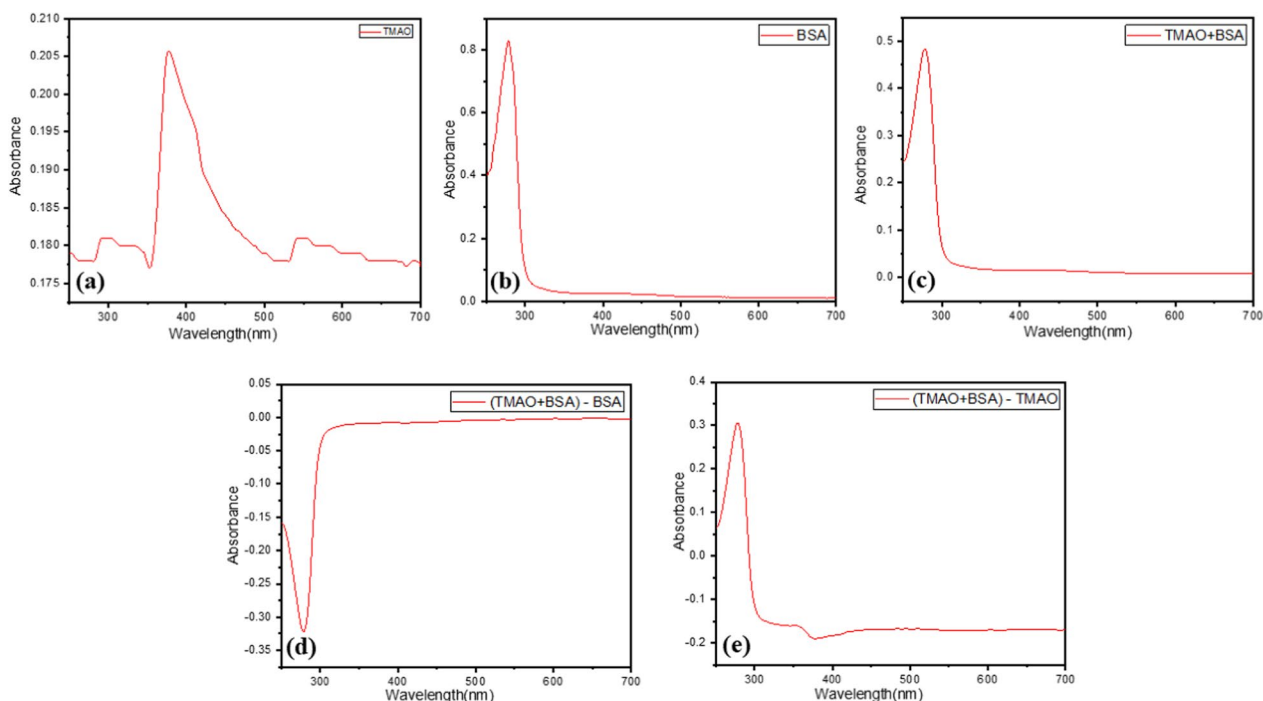


**Fig. 2** (a) UV–Vis absorbance spectra recorded for TMAO (b) in fix concentration (15  $\mu\text{M}$ ) of BSA, in acetate buffer at pH 4.3 (c) UV–vis spectra of TMAO + BSA, (d) UV–vis spectra of (TMAO + BSA)-BSA, (e) UV–vis spectra of (TMAO + BSA)-TMAO

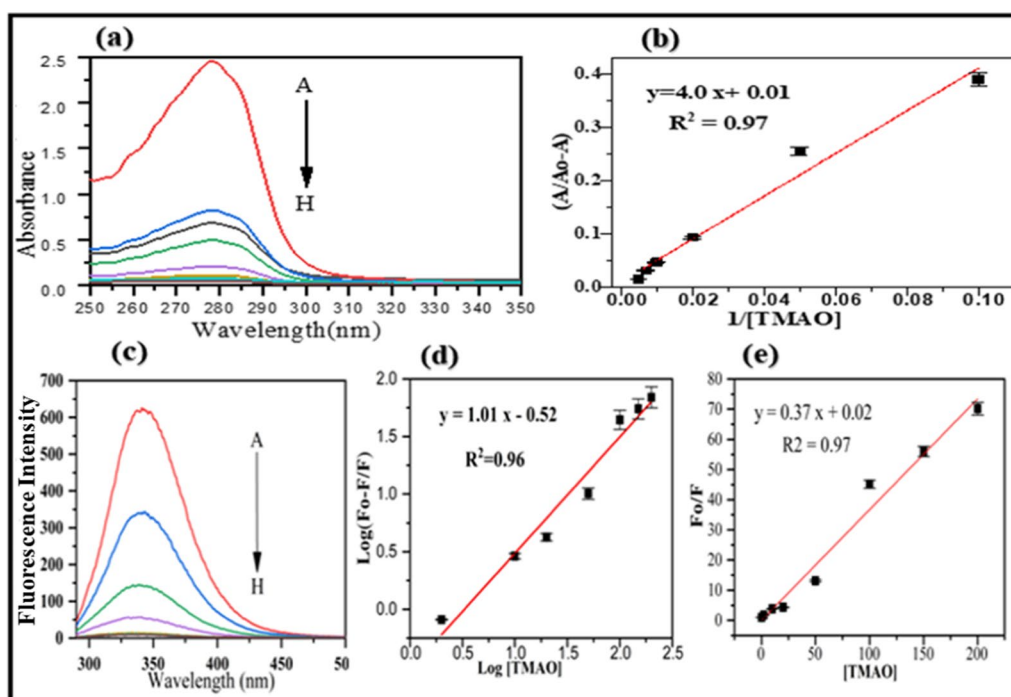


**Fig. 3** (a) UV–Vis absorbance spectra recorded for various concentration of TMAO in fix concentration (15  $\mu\text{M}$ ) of BSA, at pH 4.3 in acetate buffer, (b) Benesi–Hildebrand plot UV–Visible plot ( $A/A_0 - A$  v/s  $1/[TMAO]$ ) to calculate the total number of binding sites located on the BSA structure to associate with the TMAO, (c) Fluorescence spectra of BSA in the absence and presence of TMAO at different concentrations (2, 10, 20, 50, 100, 150 and 200  $\mu\text{M}$  respectively), and excitation wavelength were taken as 280 nm, (d) Stern Volmer (SV) plot, and (e)  $F_0/F$  v/s  $[TMAO]$

and tyrosine shows absorbance of UV light at 280 nm, which is due to presence of aromatic ring structure in their side chain R group. Delocalization of  $\pi$  electrons takes place within the aromatic ring that is responsible for the absorption of light by aromatic amino acid residues. Changes in absorbance at this wavelength typically indicate alterations in the protein's structure or environment, especially in the local environment of these aromatic residues. This could result from protein conformational changes, such as unfolding or binding interactions. Proteins absorb UV radiation proportional to the amino acid content present in it. Therefore, it is possible to quantify proteins depending upon the absorption intensity. Benesi–Hildebrand plot (Fig. 3b) was derived from the UV–Visible plot ( $A/A_0 - A$  v/s  $1/[TMAO]$ ) to calculate the total number of binding sites located on the BSA structure to associate with the metabolites. TMAO Slope of this plot gives the value of number of binding sites that is 4. The obtained values are in well agreement with the computational data.

The phenomenon of quenching of fluorescence is decrement of quantum yield of fluorophore fluorescence induced by various types of interactions at molecular level, like ground-state conjugate formation, excited-state

reactions, quenching due to collision and energy transfer [44–48]. By measuring intrinsic PL intensity of BSA protein before and after adding TMAO, there are some changes in microenvironment in proximity of fluorophore molecules. (Fig. 3c) depicts the PL spectrum of BSA in the presence of different concentrations of TMAO at room temperature. When various amount TMAO was mixed with BSA solution which is fixed in concentration, the PL intensity of BSA around 280 nm observed to be decreasing in regular pattern but  $\lambda_{\text{max}}$  (maximum emission intensity) remains unchanged to either longer or shorter wavelength.

This signifies that TMAO might have interacted with BSA and quenched its intrinsic PL intensity, but here there were not any changes observed in local dielectric micro-environment of BSA. (Fig. 3d, e) shows to Stern–Volmer (SV) plot at room temperature. Graph shows that for the given investigated range of concentrations, the SV plot shows a good linearity. The Stern–Volmer constant ( $K_{\text{sv}}$ ) may be obtained from both static as well as dynamic components. SV equation related to static quenching is formulated by taking consideration of conjugate formation between fluorophore molecule (F) and quencher molecule (Q) as reversible reaction along

with association constant ( $K$ ). But where there is dominance of static quenching, the  $K_{sv}$  may be considered to be equal to association constant ( $K$ ) between fluorophore and quencher molecule [49–51]. At low concentrations of the fluorophore, the fluorescence intensity is directly proportional to the concentration of the fluorophore [52–54]. The initial concentration of fluorophore [ $F_0$ ], is equivalent to addition of the free fluorophore concentration [ $F$ ], and no-fluorescent conjugate [ $FQ$ ]. This gives linearity for Stern–Volmer equation for static quenching.

$$\frac{F_0}{F} = 1 + K_{sv}[Q] \quad (1)$$

where  $F_0$  is the PL intensity in absence of quencher molecule, while  $F$  in the presence of quencher molecule.  $K_{sv}$  is SV quenching constant and  $[Q]$  is the quencher concentration. Here results show an excellent linear correlation between ( $F_0/F_1$ ) and  $[TMAO]$ . The coefficient  $K_{sv}$  is equal to the slope of this line; in this case, the value is 0.37.

From the above discussion it is clear that here static quenching of BSA has been occurred, induced by TMAO. The data of PL quenching of BSA protein was analyzed to find the several binding factors. The total number of binding pocket ( $n$ ) and binding constant ( $K_b$ ) may be calculated according to equation below [55].

$$\text{Log} \left[ \frac{F_0 - F}{F} \right] = \log K_b + n \log [Q] \quad (2)$$

Here  $F_0$  and  $F$  are fluorescent intensities in absence and presence of quencher molecule in steady state. From the Eq. (2), values of  $n$  and  $K_b$  at room temperature were obtained to be 1.01 and 0.28 respectively. This implies that TMAO molecule is strongly bound to BSA. Also, here there is one independent class of binding pocket for TMAO molecule towards BSA. The linear-coefficient ( $R$ ) is 0.96 which indicates that the underlying assumptions of derivation for Eq. (2) was satisfactory.

To determine the interaction force between TMAO and BSA protein, the signs as well as magnitudes of the thermodynamic parameter ( $\Delta G$ ) are accountable for the main interaction forces involved in binding process. The force of interaction between ligands and bio-macromolecules includes multiple hydrogen bonds, hydrophobic interaction, electrostatic interactions and van der Waals forces etc. Change in free energy ( $\Delta G$ ) was further estimated from the equation mentioned below:

$$\Delta G = -RT \ln K_b \quad (3)$$

where  $K_b$  and  $R$  represents binding constant and gas constant (8.314 J/Mol/K) respectively.

In their landmark study, Ross and Subramaniam emphasize that understanding binding interactions requires a detailed analysis of both enthalpy ( $\Delta H$ ) and entropy ( $\Delta S$ ), rather than focusing solely on the free energy change ( $\Delta G$  in kJ/mol)). These parameters reveal the fundamental forces driving interactions. Enthalpy ( $\Delta H$  in kJ/mol) indicates the nature of bonding forces involved, such as hydrogen bonding, van der Waals interactions, and electrostatic forces. When  $\Delta H$  is negative, it typically suggests that favorable interactions, like hydrogen bonds or ionic interactions, are predominant. Entropy ( $\Delta S$  in J/(mol·K)) sheds light on changes in molecular order, particularly in solvent structure and protein flexibility. Positive entropy often signifies increased disorder, such as solvent molecules being released from the binding interface, favoring hydrophobic interactions. Free Energy ( $\Delta G$ ) alone provides the net spontaneity of the reaction but not the interaction specifics. Therefore, dissecting  $\Delta G$  into  $\Delta H$  and  $T\Delta S$  components allows for a precise understanding of whether enthalpic or entropic contributions dominate the binding process. Ross and Subramaniam argue that examining both enthalpy and entropy changes are crucial for accurately characterizing the interaction forces between molecules like TMAO and BSA, as each parameter offers unique insights into the binding dynamics.

The negative value of  $\Delta G$  indicates the spontaneity of the reaction between metabolite and BSA. The negative value of  $\Delta G$  ( $-3.15$  kJ/mol) revealed that binding process is spontaneous.

A binding energy (or  $\Delta G$  for binding) of  $-3.15$  kJ/mol represents a weak interaction between molecules. The magnitude of binding energy i.e.  $\Delta G$  values around  $-3$  to  $-5$  kJ/mol suggest weak, reversible interactions like van der Waals forces or hydrogen bonding.  $-3.15$  kJ/mol suggests that the interaction is weak and likely reversible, meaning the molecules involved will associate and dissociate frequently. A binding energy of  $-3.15$  kJ/mol suggests the interaction is relatively weak in a biological system. Weak binding may be useful for transient interactions but may not sustain the stable association necessary for complex formation or sustained activity. Moreover, the weak interaction supports the elimination of the metabolite from the body so that the physiological range of metabolite is maintained in the body.

#### CD study

To observe the secondary structural change in BSA protein after interacting with ligand molecule, circular dichroism spectroscopy technique was used [56]. Figure 4 shows the CD spectrum of the BSA interaction with different concentration (2, 10, 20, 50, 100, 150, and 200  $\mu\text{M}$  respectively) of the TMAO in acetate buffer

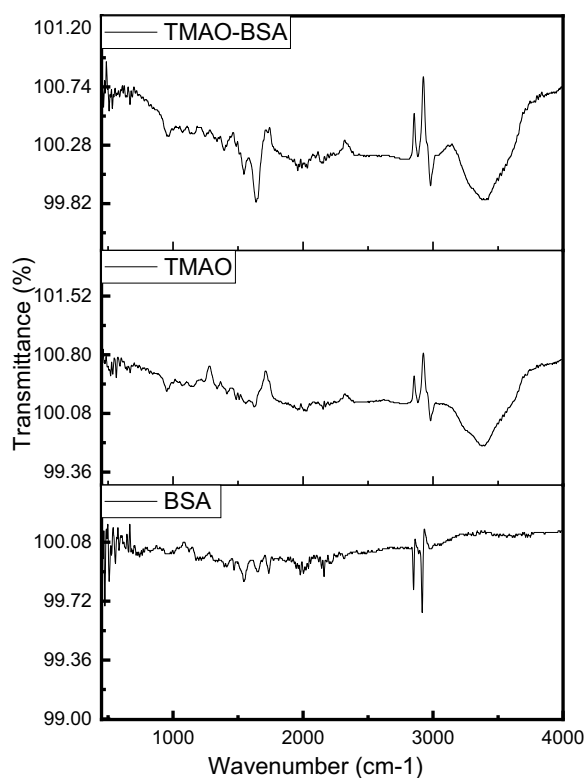
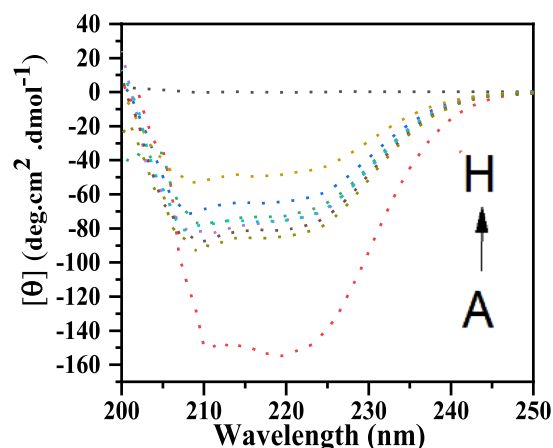


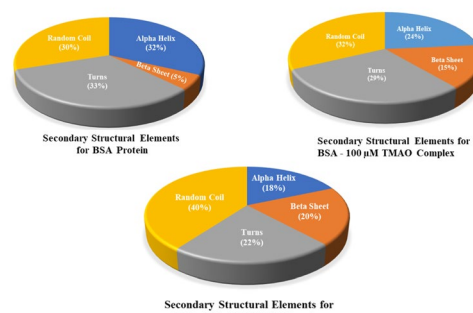
**Fig. 4** FTIR spectra of BSA recorded in the presence and absence of TMAO at various concentration

pH=4.3 at room temperature. Figure 4 clearly shows that BSA is exhibiting two negative peaks, one at 208 nm and other at 222 nm in ultraviolet zone, which is characteristic of typical  $\alpha$ -helix structure of BSA protein. Both peaks at 208 nm as well as 222 nm contribute towards  $n \rightarrow \pi^*$  transition for the given peptide bonds of  $\alpha$ -helices. As the concentration of TMAO is increased here, the intensity curves of given decreases in regular pattern from A–H (Fig. 5a, band intensity curves A–H). The CD spectra of BSA protein were taken in the presence as well as in absence of TMAO that are showing similar shape of BSA indicating that BSA structure is still predominating the  $\alpha$ -helices (32%).

As we know BSA is sensitive to pH, which can induce conformational changes affecting its secondary structure. BSA typically maintains a high  $\alpha$ -helical content under physiological pH, i.e., close to neutral pH, but acidic or basic environments can partially unfold the protein, decreasing the  $\alpha$ -helix content. Denaturation at lower pH levels is well-documented, where BSA may transition to partially unfolded states to less  $\alpha$ -helical structure [57]. Acidic pH induces protonation, which disrupts hydrogen bonds and can lower  $\alpha$ -helix stability. The major decrease in ellipticity is related to a decrease in the percentage of alpha helix shown in Fig. 5b confirming the interaction



(a)



(b)

**Fig. 5** (a) CD spectra of BSA recorded in the presence and absence of TMAO at various concentration (2, 10, 20, 50, 100, 150, and 200  $\mu$ M respectively); (A in Red colour represents BSA having 15  $\mu$ M concentration, B to G various concentrations of TMAO mention colorwise), (b) Pie chart of secondary structural elements calculated from CD spectra of BSA (15  $\mu$ M) recorded in the presence and absence of TMAO at various concentration showing the % decrease in alpha helix)

of TMAO with BSA. The same has been computationally validated (Fig. 8) as the major types of amino acids present in alpha helix contributing to interaction with TMAO.

#### FTIR

To confirm the interaction between TMAO-BSA conjugate, the FTIR spectral analysis was used. The compositions of pure BSA, TMAO dissolved in acetate buffer pH=4.3, and TMAO-BSA conjugate were tested separately. Figure 4 shows the comparison of the FTIR spectra for pure BSA, TMAO in acetate buffer and TMAO-BSA conjugate [58, 59] (Table 1).

There are few peaks in the fingerprint region from 900 to 1650  $\text{cm}^{-1}$  which were present in all three spectra

**Table 1** Transmission peaks in FTIR and their respective assignment in BSA, TMAO and TMAO-BSA conjugate

Wavenumber (cm <sup>-1</sup> )	Assigned To	TMAO	BSA	TMAO + BSA
956	C–C bond out of the plane deformation	√	√	√
1075	C–OH stretch	√ (due to acetate buffer)	√	√
1146	C–N bending	√	–	√
1243	N–O in N-Oxides	√	–	√
1344	N–H and C–H in-plane deformation	√	√	√
1400	C–N stretching vibration	√	√	√
1465	CH <sub>3</sub> deformation stretch	–	√	–
1548	N–H in aliphatic nitro compounds	–	√	√
1640	C=O stretch	–	√	√
1656	NH bending	–	√	√
1735	C=O stretch	–	√	√
1964	C=C Antisymmetric Stretch	√	√	√
2030	N – H deformation stretch	√	√	√
2150	N–C Stretch	√	√	√

corresponding to C–OH, C–N and COO<sup>-</sup> groups that are due to both BSA and TMAO. The CH stretch in aliphatic compounds appeared between 2800 and 3000 cm<sup>-1</sup> which were present in all three spectra. The broad peaks appeared above 3000 cm<sup>-1</sup> correspond to OH and NH stretch vibrations. Further, the characteristic amide I and II bands in BSA appeared at 1640, 1656 and 1548 cm<sup>-1</sup> respectively. There is no change in the peak position of the amide I appeared suggesting the BSA structure is not destroyed which was confirmed from CD results also. Thus, FTIR spectrum confirmed the formation of conjugation between TMAO and BSA.

### Contact angle

To know the hydrophobic or hydrophilic nature of TMAO-BSA complex the measurement of contact angle of BSA, TMAO and conjugates (BSA: TMAO) were carried out on ELISA plate. BSA protein is both hydrophobic as well as hydrophilic in nature. The hydrophilicity of BSA is mainly contributed due to lysine amino acid residue that contains positively charged amino group. Also arginine, glutamine, and asparagine have polar or charged side chains that may interact favorably with water molecules through hydrogen bonding and electrostatic interactions, making them hydrophilic. Amino acids with hydroxyl groups like serine and threonine and amino acids with amide groups such as asparagine and glutamine also contribute to the hydrophilic nature of BSA. The hydrophobic nature of BSA protein is primarily due to the presence of amino acids with nonpolar side chains, like alanine, valine, leucine, isoleucine, phenylalanine, and tryptophan. These amino acids have

hydrophobic characteristics because their side chains lack charged or polar groups, making them unable to form favorable interactions with water molecules. Among these, amino acids like leucine, isoleucine, phenylalanine, and tryptophan are particularly hydrophobic due to the presence of bulky hydrocarbon side chains. These hydrophobic amino acids tend to cluster together in the interior of the protein's structure, away from the surrounding water molecules, contributing to the overall hydrophobicity of BSA. When the hydrophobic BSA bind with other ligands like TMAO, the surface wettability changes which can be evaluated using contact angle measurement studies. The protein–ligand interaction alters the contact angles. Due to binding between them, a decrease in contact angle can be observed due to the increase in the hydrophilicity of the protein. Here the contact angle formed by BSA molecules with ELISA plate is 91°, that means here it is involved in hydrophobic-hydrophobic interaction with the plate surface in acetate buffer solution. TMAO is amphiphilic molecule in nature as it has both hydrophilic and hydrophobic moieties [60]. Subsequently,  $\theta$  value for TMAO was also checked, which is less i.e., 82.95° in comparison with BSA. This suggests the TMAO molecules form stronger bond with plate surface in comparison to the TMAO in acetate buffer. Thereafter, when TMAO was allowed to form conjugate with BSA molecules in different ratios from 1:1 to 1:100; the  $\theta$  value continuously decreased with the increasing ratio, respectively as shown in Fig. 6a–h.

The hydrophilic nature of TMAO is due to its polar group which interacts with water molecule. When TMAO combines with BSA the resulting conjugate becomes more hydrophilic as observed from the above

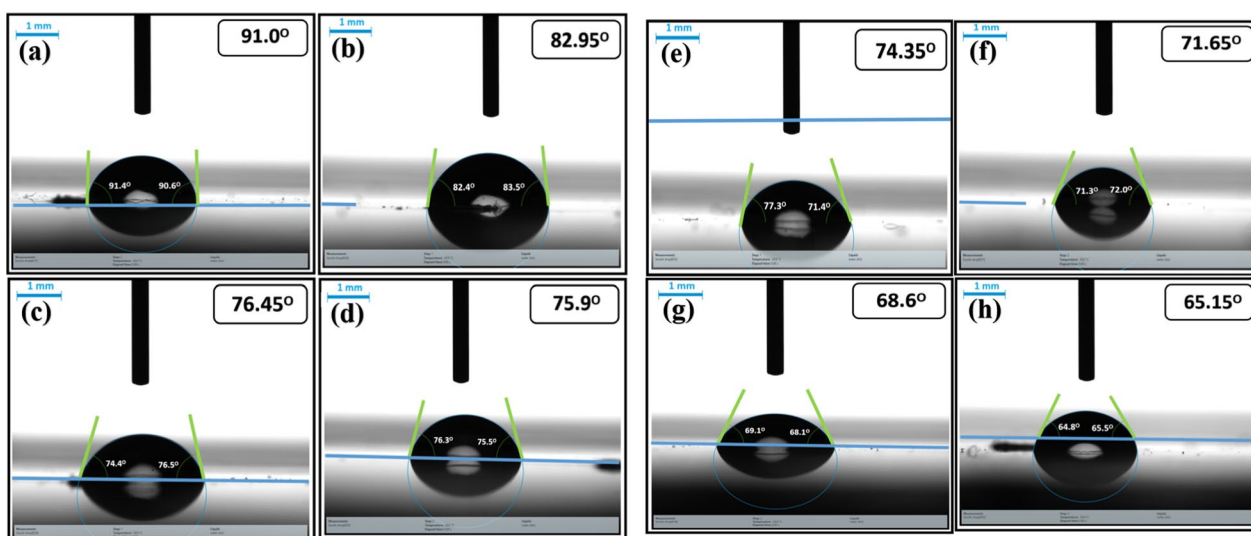


**Fig. 6** (a–h) Contact angle of BSA and of TMAO-BSA conjugate at various concentration of TMAO

results. TMAO has been observed to stabilize proteins and maintain their solubility due to ability of forming hydrogen bonds with water molecules and protein surfaces. So the combination of TMAO with BSA is expected to enhance the hydrophilic nature of the TMAO-BSA conjugate.

## Docking results

### Theoretical modeling of TMAO and DFT

Using Marvin Sketch and ChemBioDraw Ultra, we generated a 3D model of TMAO, confirming structural accuracy through 3D cleaning and visualization. Key parameters, including atomic coordinates, bond lengths (shown in Table S1), and angles (shown in , were

calculated, with successive energy minimization steps performed to stabilize the structure. Final optimization to the lowest energy state was achieved via DFT calculations with Gaussian 09, applying the 6-311G basis set and RB3LYP functional for high precision. Figure 7a shows the ground state configuration of TMAO as the space-filling model after optimization as well as energy minimization. The energy value of optimized molecule was found to be  $E = -249.68522468$  a.u., while RMS Gradient Norm = 0.00830651 a.u. with dipole moment = 4.6272 debye. The greyish color balls represent carbon atoms, white color ball hydrogen atoms, while ball with blue color symbolizes nitrogen atom, and pink color represent oxygen atoms of TMAO molecule.

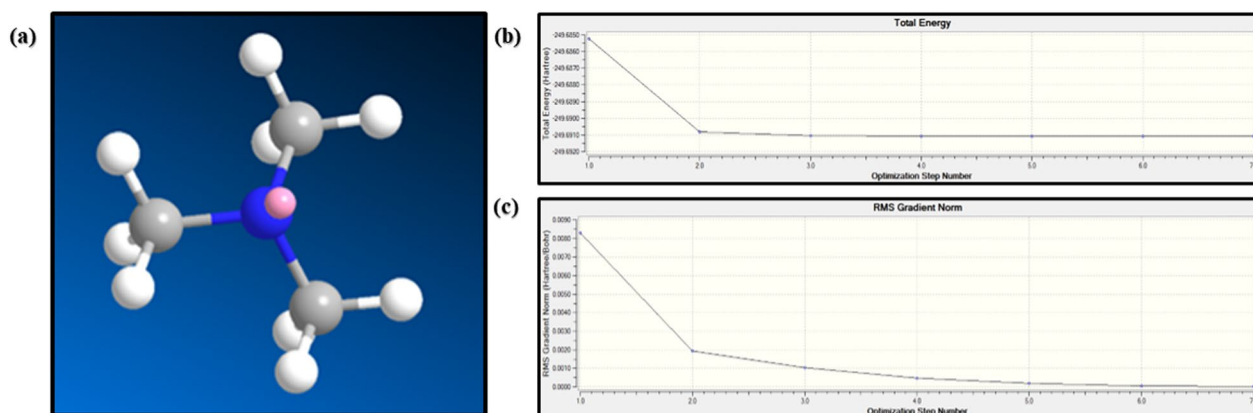


**Fig. 7** (a) 3D structure of ground state configuration of TMAO molecule, drawn using Marvin Sketch, (b) Energy minimization and optimization graph of TMAO showing energy minimization with optimization step number using Chem DrawPro, ChemBioDraw Ultra and Gaussian 09, (c) Energy minimization and optimization graph of TMAO showing energy RMS gradient normalization with optimization step number using ChemBioDraw Ultra and Gaussian 09

The different bond lengths (in Å) and bond angles (°) for all possible confirmations of atoms present in TMAO molecule in 3D space has been mentioned in detail in table S1 and table S2 respectively.

#### Docking of TMAO with BSA

HIS 67 and GLU 243 were observed to be involved in conventional hydrogen bond formation with TMAO.

GLU 243, ASP 248 and GLU 251 are involved in electrostatic interaction while LYS 242 is involved in carbon hydrogen bond as shown in Fig. 8. From docking result, it is clearly shown that the TMAO is binding with BSA. Since the TMAO is very small molecule so interaction is weak here as evident from the binding energy score value is  $-3.6$  kcal/mol (shown in Table S3).

#### MD simulation and MMGBSA of TMAO with BSA

The BSA protein and TMAO ligand RMSD value is mentioned in Fig. S1 for 150 ns simulation. The ligand RMSD is little fluctuating, that means TMAO is found to be in

the binding pocket of the protein but on the surface of the protein. In addition, the RMSD of BSA is not fluctuating, so overall structure of protein remains relatively stable after binding with TMAO in TMAO-BSA complex.

A timeline representation of the interactions and contacts of TMAO with BSA has been monitored throughout the simulation until 150 ns (Fig. S2). The top panel shows the total number of specific contacts the protein makes with the ligand over the course of the trajectory. The bottom panel shows which residues interact with the ligand in each trajectory. Some residues make more than one specific contact with the ligand, which is represented by a darker shade of orange, according to the scale to the right of the plot. In our research, mainly four types of interaction like hydrogen bonds, hydrophobic, ionic and water bridges have been observed in TMAO-BSA complex as shown in the plot above in the Fig. 9. Each interaction type contains subtypes that are more specific. The stacked bar charts are normalized over the course of the trajectory. Values over 1.0 are possible as some protein residue may make multiple contacts of same subtype with

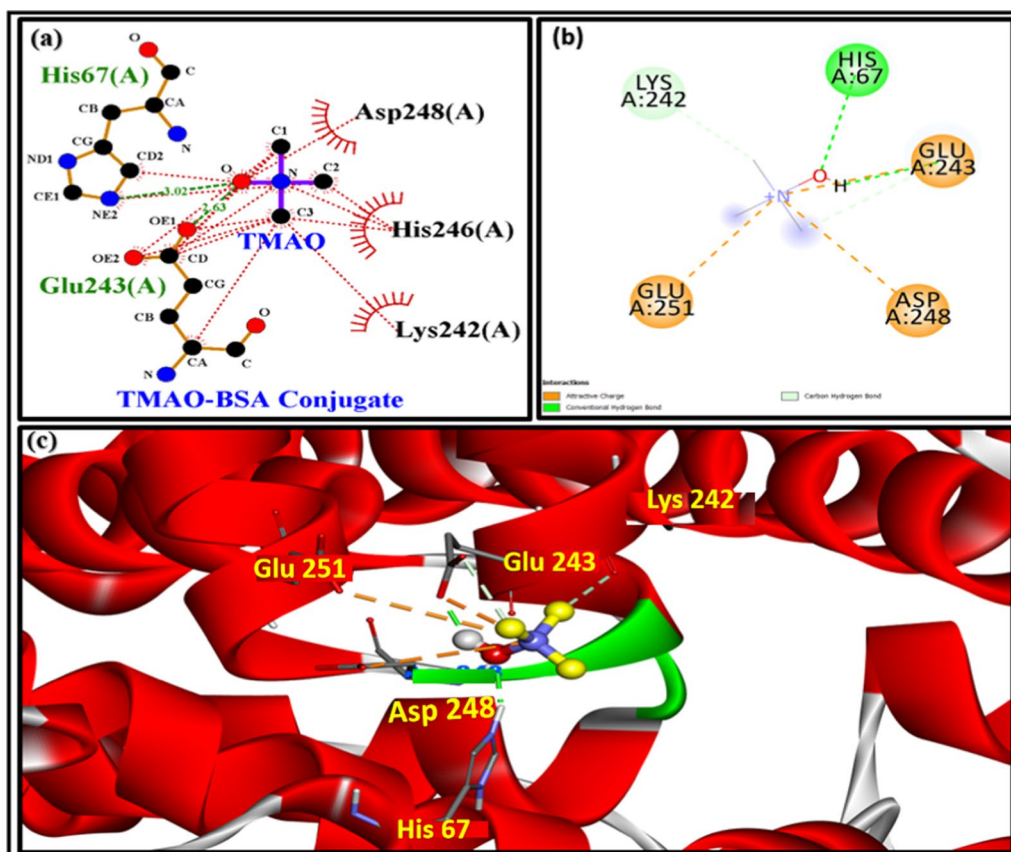


**Fig. 8** shows the TMAO-BSA docked complex, having involvement of electrostatics and hydrogen bonding of TMAO with BSA (a) shows the ligand plot structure of interaction of different amino acid residues with different atoms of TMAO, (b) 2D interactions, and (c) 3D interaction of TMAO-BSA conjugate

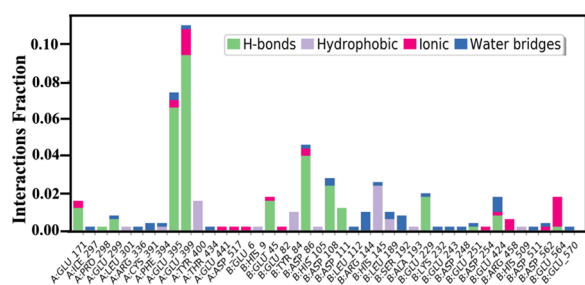


**Fig. 9** shows the involvement of amino acid residue of BSA in TMAO-BSA complex, having involvement of electrostatics and hydrogen, hydrophobic interaction and water bridges

the TMAO molecule. Consideration of hydrogen-bonding properties in TMAO-BSA interaction is important because of their strong influence on specificity, metabolism and adsorption. Hydrogen bonds between TMAO and BSA are backbone acceptor; backbone donor; side-chain acceptor, and side-chain donor. Hydrophobic interactions are either  $\pi$ -Cation;  $\pi$ - $\pi$ ; or non-specific interactions. Ionic interactions are between two oppositely charged atoms that are within 3.7 Å of each other and do not involve a hydrogen bond. Water Bridges are hydrogen-bonded protein–ligand interactions mediated by a water molecule. A schematic of detailed interactions of TMAO atoms with the BSA amino acid residues, that occur more than 30.0% of the simulation time in the selected trajectory for 150.30 nsec, are shown. It is possible to interact with >100% as some residues may have multiple interactions of a single type with the same ligand atom. The  $\Delta G$  calculated through MMGBSA was found to be more negative which suggests that TMAO is binding with BSA forming TMAO-BSA complex.

## Conclusion

This manuscript describes about the interaction of TMAO with BSA with the help of various optical techniques and computational methods that are in well agreement with each other. UV–Vis absorbance spectroscopy indicated the decrease in absorbance of BSA with the increasing concentration of TMAO, which could mainly be due to TMAO-BSA conjugate formation. Fluorescence quenching in emission spectrum of BSA upon addition of increasing concentration of TMAO confirms the conjugate formation. The occurrence of static quenching was confirmed via Stern–Volmer (SV) plot, which also supported the conjugate formation. *In silico* analysis, i.e. molecular docking, MD simulation and MM/GBSA, concluded that four major types of interactions like hydrogen bonding, electrostatic interaction, hydrophobic interactions and water

bridges are the major factors for stabilizing the TMAO-BSA complex, with a binding energy of  $-3.6$  kcal/mol. The  $\Delta G$  calculated through MM/GBSA was found to be negative that reveals TMAO-BSA complex formation is a spontaneous process. TMAO-serum albumins interaction studies could be helpful in screening aptamer against TMAO that could further be helpful in early diagnosis of the diseases such as metabolic, cardiovascular, colorectal cancer and, neurological disorders.

## Abbreviations

TMAO	Trimethylamine-N-oxide
BSA	Bovine serum albumin
HSA	Human serum albumin
NF- $\kappa$ B	Nuclear factor kappa-light-chain-enhancer of activated B cells
MAPK	Mitogen-activated protein kinase
ROS	Reactive oxygen species
T2DM	Type 2 diabetes mellitus
TNF- $\alpha$	Tumor necrosis factor-alpha
IL-6	Interleukin-6
CKD	Chronic kidney disease
MM/GBSA	Molecular mechanics/generalized born surface area
CD	Circular dichroism
FTIR	Fourier-transform infrared spectroscopy
DFT	Density functional theory
UV–vis	Ultraviolet–visible spectroscopy
HEWL	Hen egg white lysozyme
BHb	Bovine hemoglobin
4-EPS	4-Ethyl Phenyl Sulfate

## Supplementary Information

The online version contains supplementary material available at <https://doi.org/10.1186/s13065-024-01375-0>.

Additional file 1

## Acknowledgements

The authors acknowledge funding support from core grant received from the National Institute of Immunology, New Delhi. Authors would also acknowledge the SCFBio IIT Delhi and School of Bioengineering and Biosciences LPU, for providing the computational facility.

## Author contributions

AKV has performed experiments, analyzed the data and wrote the manuscript. PG has helped in experimental work. AM and NR have edited the manuscript and provided the support for MD simulation. GBVS has helped in FTIR data analysis as well as reviewed the draft of manuscript. AK and PS conceptualized and designed the work and edited the manuscript to its final shape. AK supervised the whole project.

## Funding

Core Grant: National Institute of Immunology, India.

## Availability of data and materials

All data and materials related to this study are available upon reasonable request.

## Declarations

### Ethics approval and consent to participate

All the experiments were conducted following the ethical approval (IBSC#508/22) and recommendation issued by the Institutional Biosafety Committee (IBSC) of the National Institute of Immunology, New Delhi.

**Consent for publication**

Not applicable.

**Competing interests**

The authors declare no competing interests.

Received: 29 September 2024 Accepted: 27 December 2024

Published online: 21 January 2025

**References**

1. Zeisel SH, Warrier M. Trimethylamine N-oxide, the microbiome, and heart and kidney disease. *Annu Rev Nutr.* 2017;37:157–81. <https://doi.org/10.1146/annurev-nutr-071816-064732>.
2. Subramaniam S, Fletcher C. Trimethylamine N-oxide: breathe new life. *Br J Pharmacol.* 2018;175(8):1344–53. <https://doi.org/10.1111/bph.13959>.
3. Jalandra R, et al. Emerging role of trimethylamine-N-oxide (TMAO) in colorectal cancer. *Appl Microbiol Biotechnol.* 2021;105(20):7651–60. <https://doi.org/10.1007/s00253-021-11582-7>.
4. Ronen D, et al. Human gut microbiota in cardiovascular disease. *Compr Physiol.* 2024;14(3):5449–90. <https://doi.org/10.1002/cphy.c230012>.
5. Holle J, et al. Gut dysbiosis contributes to TMAO accumulation in CKD. *Nephrol Dial Transplant.* 2024;39(11):1923–6. <https://doi.org/10.1093/ndt/gfae152>.
6. Yancey PH. Trimethylamine N-oxide (TMAO): a unique counteracting osmolyte? *Paracelsus Proc Exp Med.* 2023;2(S1):67–91. <https://doi.org/10.33594/000000661>.
7. Hu CY, Lynch GC, Kokubo H, Pettitt BM. Trimethylamine N-oxide influence on the backbone of proteins: an oligoglycine model. *Proteins.* 2010;78(3):695–704. <https://doi.org/10.1002/prot.22598>.
8. Ufnal M, Zadlo A, Ostaszewski R. TMAO: a small molecule of great expectations. *Nutrition.* 2015;31(11–12):1317–23. <https://doi.org/10.1016/j.nut.2015.05.006>.
9. Su Z, Dias CL. Individual and combined effects of urea and trimethylamine N-oxide (TMAO) on protein structures. *J Mol Liq.* 2019;293:111443. <https://doi.org/10.1016/j.molliq.2019.111443>.
10. Ma J, Pazos IM, Gai F. Microscopic insights into the protein-stabilizing effect of trimethylamine N-oxide (TMAO). *Proc Natl Acad Sci USA.* 2014;111(23):8476–81. <https://doi.org/10.1073/pnas.1403224111>.
11. Liao YT, Manson AC, DeLyser MR, Noid WG, Cremer PS. Trimethylamine N-oxide stabilizes proteins via a distinct mechanism compared with betaine and glycine. *Proc Natl Acad Sci USA.* 2017;114(10):2479–84. <https://doi.org/10.1073/pnas.1614609114>.
12. Yancey PH. Organic osmolytes as compatible, metabolic and counteracting cytoprotectants in high osmolarity and other stresses. *J Exp Biol.* 2005;208(15):2819–30. <https://doi.org/10.1242/jeb.01730>.
13. Li X, Yang Z. Interaction of oridonin with human serum albumin by isothermal titration calorimetry and spectroscopic techniques. *Chem Biol Interact.* 2015;232:77–84. <https://doi.org/10.1016/j.cbi.2015.03.012>.
14. Bi S, et al. Investigation of the interaction between flavonoids and human serum albumin. *J Mol Struct.* 2004;703(1–3):37–45. <https://doi.org/10.1016/j.molstruc.2004.05.02>.
15. Michnik A, Michalik K, Kluczevska A, Drzazga Z. Comparative DSC study of human and bovine serum albumin. *J Therm Anal Calorim.* 2006;84(1):113–7. <https://doi.org/10.1007/s10973-005-7170-1>.
16. Kamali A, Jahmide-Azizi N, Oliva R, Winter R. Deep sea osmolytes in action: their effect on protein-ligand binding under high pressure stress. *Phys Chem Chem Phys.* 2022;24(30):17966–78. <https://doi.org/10.1039/d2cp01769e>.
17. Courtenay ES, Capp MW, Anderson CF, Record MT. Vapor pressure osmometry studies of osmolyte–protein interactions: implications for the action of osmoprotectants in vivo and for the interpretation of osmotic stress experiments in vitro. *Biochemistry.* 2000;39(15):4455–71. <https://doi.org/10.1021/bi992887l>.
18. Sugio S, Kashima A, Mochizuki S, Noda M, Kobayashi K. Crystal structure of human serum albumin at 2.5 Å resolution. *Protein Eng.* 1999;12(6):439–46. <https://doi.org/10.1093/protein/12.6.439>.
19. Tang WHW, et al. Intestinal microbial metabolism of phosphatidylcholine and cardiovascular risk. *N Engl J Med.* 2013;368(17):1575–84. <https://doi.org/10.1056/NEJMoa1109400>.
20. Yue Y, Liu J, Fan J, Yao X. Binding studies of phloridzin with human serum albumin and its effect on the conformation of protein. *J Pharm Biomed Anal.* 2011;56(2):336–42. <https://doi.org/10.1016/j.jpba.2011.05.018>.
21. Seedher N, Agarwal P. Complexation of fluoroquinolone antibiotics with human serum albumin: A fluorescence quenching study. *J Lumin.* 2010;130(10):1841–8. <https://doi.org/10.1016/j.jlumin.2010.04.020>.
22. Chaves OA, et al. Fluorescence and docking studies of the interaction between human serum albumin and pheophytin. *Molecules.* 2015;20(10):19526–39. <https://doi.org/10.3390/molecules201019526>.
23. Gulati P, Kumar Verma A, Kumar A, Solanki P. Para-cresyl sulfate and BSA conjugation for developing aptasensor: spectroscopic methods and molecular simulation. *ECS J Solid State Sci Technol.* 2023;12(7):73004. <https://doi.org/10.1149/2162-8777/ace286>.
24. Li S, Tonelli M, Unsworth LD. Indoxyl and p-cresol sulfate binding with human serum albumin. *Colloids Surfaces A Physicochem Eng Asp.* 2022;635:128042. <https://doi.org/10.1016/j.colsurfa.2021.128042>.
25. Sulkowska A. Interaction of drugs with bovine and human serum albumin. *J Mol Struct.* 2002;614(1–3):227–32. <https://doi.org/10.1021/jf201796x>.
26. Zhang Y, Shi S, Chen X, Zhang W, Huang K, Peng M. Investigation on the interaction between ilaprazole and bovine serum albumin without or with different C-ring flavonoids from the viewpoint of food–drug interference. *J Agric Food Chem.* 2011;59(15):8499–506. <https://doi.org/10.1021/jf201796x>.
27. Das S, Sarmah S, Roy AS. Monitoring fluorescence emission behaviors of dietary polyphenols in a serum albumin environment. *New J Chem.* 2020;44(2):299–302. <https://doi.org/10.1039/C9NJ03938D>.
28. Lv Y, Liang Q, Li Y, Liu X, Zhang D, Li X. Study of the binding mechanism between hydroxytyrosol and bovine serum albumin using multispectral and molecular docking. *Food Hydrocoll.* 2022;122:107072. <https://doi.org/10.1016/j.foodhyd.2021.107072>.
29. Gu J, Yang G, Li X, He Q, Huang X, Sun T. Difference in the binding mechanism of distinct antimony forms in bovine serum albumin. *Biomaterials.* 2021;34:493–510. <https://doi.org/10.1007/s10534-021-00291-3>.
30. Das S, et al. Lysozyme–luteolin binding: molecular insights into the complexation process and the inhibitory effects of luteolin towards protein modification. *Phys Chem Chem Phys.* 2019;21(23):12649–66. <https://doi.org/10.1039/C9CP01128E>.
31. Das S, et al. Targeting the heme protein hemoglobin by (–)-epigallocatechin gallate and the study of polyphenol–protein association using multi-spectroscopic and computational methods. *Phys Chem Chem Phys.* 2020;22(4):2212–28. <https://doi.org/10.1039/C9CP05301H>.
32. Gulati P, Solanki P, Verma AK, Kumar A. Interaction of 4-ethyl phenyl sulfate with bovine serum albumin: Experimental and molecular docking studies. *PLoS ONE.* 2024;19(10):e0309057. <https://doi.org/10.1371/journal.pone.0309057>.
33. Kumar S, et al. Computational frontiers in aptamer-based nanomedicine for precision therapeutics: a comprehensive review. *ACS Omega.* 2024;9(25):26838–62. <https://doi.org/10.1021/acsomega.4c02466>.
34. Yancey PH, Clark ME, Hand SC, Bowlus RD, Somero GN. Living with water stress: evolution of osmolyte systems. *Science.* 1982;217(4566):1214–22. <https://doi.org/10.1126/science.7112124>.
35. Peters T. All about albumin. *Biochemistry, genetics, and medical applications.* Genet Med Appl. 1996. <https://doi.org/10.1093/clinchem/43.10.2014a>.
36. Hong J, Xiong S. TMAO–protein preferential interaction profile determines TMAO's conditional in vivo compatibility. *Biophys J.* 2016;111(9):1866–75. <https://doi.org/10.1016/j.bpj.2016.09.035>.
37. Zhang YZ, Xiang X, Mei P, Dai J, Zhang LL, Liu Y. Spectroscopic studies on the interaction of Congo Red with bovine serum albumin. *Spectrochim Acta—Part A Mol Biomol Spectrosc.* 2009;72(4):907–14. <https://doi.org/10.1016/j.saa.2008.12.007>.
38. Bastyns K, Froeyen M, Díaz JF, Volckaert G, Engelborghs Y. Experimental and theoretical study of electrostatic effects on the isoelectric pH and the pKa of the catalytic residue His-102 of the recombinant ribonuclease from *Bacillus amyloliquefaciens* (barnase). *Proteins Struct Funct Bioinforma.* 1996;24(3):370–8. [https://doi.org/10.1002/\(SICI\)1097-0134\(199603\)24:3%3c370::AID-PROT10%3e3.0.CO;2-J](https://doi.org/10.1002/(SICI)1097-0134(199603)24:3%3c370::AID-PROT10%3e3.0.CO;2-J).

39. Theng BKG. Proteins and enzymes. In: Formation and properties of clay-polymer complexes, vol. 4. Amsterdam: Elsevier; 2012. p. 245–318.
40. Verma AK, Sharma S, Jayaraj A, Deep S. In silico study of interaction of (ZnO) 12 nanocluster to glucose oxidase-FAD in absence and presence of glucose. *J Biomol Struct Dyn*. 2023. <https://doi.org/10.1080/07391102.2023.2188431>.
41. Majorek KA, et al. Structural and immunologic characterization of bovine, horse, and rabbit serum albumins. *Mol Immunol*. 2012;52(3):174–82. <https://doi.org/10.1016/j.molimm.2012.05.011>.
42. Verma AK, Mishra A, Kumar T, Sardar M, and Solanki PR. Experimental and In Silico interaction studies of Alpha Amylase-Silver nanoparticle: a nano-bio-conjugate. pp. 1–17, 2022. <https://doi.org/10.1101/2022.06.11.495728>.
43. Genheden S, Ryde U. The MM/PBSA and MM/GBSA methods to estimate ligand-binding affinity. *Expert Opin Drug Discov*. 2015;10(5):449–61. <https://doi.org/10.1517/17460441.2015.1032936>.
44. Wang YQ, Zhang HM, Zhang GC, Tao WH, Tang SH. Interaction of the flavonoid hesperidin with bovine serum albumin: a fluorescence quenching study. *J Lumin*. 2007;126(1):211–8. <https://doi.org/10.1016/j.jlumin.2006.06.013>.
45. Verma AK. ZnO quantum dots a novel nanomaterial for various applications: recent advances and challenges. *Ind J Biochem Biophys*. 2022;59(12):1190–8. <https://doi.org/10.56042/ijbb.v59i12.67314>.
46. Verma AK. Application of fluorescence quantum dots to understand the interaction between nanomaterials and biomolecules. <http://hdl.handle.net/10603/332343>.
47. Verma AK, Ansari ZA. Fluorescent ZnO quantum dot probe to study glucose-glucose oxidase interaction via fluorescence resonance energy transfer. *Sens Lett*. 2020;18(5):351–65. <https://doi.org/10.1166/sl.2020.4232>.
48. Verma AK, Dhiman TK, Lakshmi G, Solanki P. Optical tuning of polymer functionalized zinc oxide quantum dots as a selective probe for specific detection of antibiotics. *BioRxiv*. 2022. <https://doi.org/10.1101/2022.11.04.515220>.
49. Skotheim TA. Conjugated polymers: theory, synthesis, properties, and characterization, 3rd ed. 2006. <https://doi.org/10.1201/9781420043594>.
50. Acquavella MF, Evans ME, Farraher SW, Névoret CJ, Abelt CJ. Static and dynamic fluorescence quenching of a dicyanoanthracene-capped  $\beta$ -cyclodextrin. *J Chem Soc, Perkin Trans*. 1995;2(2):385–8. <https://doi.org/10.1039/p29950000385>.
51. Lakowicz JR. Principles of fluorescence spectroscopy, Third Edition. Springer Science. 2006; pp. 954.
52. Lakowicz JR. Introduction to fluorescence BT. In: Principles of fluorescence spectroscopy. Springer; 1999. p. 1–23. [https://doi.org/10.1007/978-0-387-46312-4\\_2](https://doi.org/10.1007/978-0-387-46312-4_2).
53. Fonin AV, Sulatskaya AI, Kuznetsova IM, Turoverov KK. Fluorescence of dyes in solutions with high absorbance. Inner filter effect correction. *PLoS ONE*. 2014. <https://doi.org/10.1371/journal.pone.0103878>.
54. Choi Y-J, Sawada K. Physical sensors: fluorescence sensors. Oxford: Elsevier; 2023. p. 1–19. <https://doi.org/10.1016/B978-0-12-822548-6.00095-9>.
55. Kang J, Liu Y, Xie MX, Li S, Jiang M, Wang YD. Interactions of human serum albumin with chlorogenic acid and ferulic acid. *Biochim Biophys Acta—Gen Subj*. 2004;1674(2):205–14. <https://doi.org/10.1016/j.bbagen.2004.06.021>.
56. Haq SK, Khan RH. Spectroscopic analysis of thermal denaturation of *Cajanus cajan* proteinase inhibitor at neutral and acidic pH by circular dichroism. *Int J Biol Macromol*. 2005;35(1–2):111–6. <https://doi.org/10.1016/j.ijbiomac.2004.12.005>.
57. Bujacz A. Structures of bovine, equine and leporine serum albumin. *Acta Crystallogr D Biol Crystallogr*. 2012;68(Pt 10):1278–89. <https://doi.org/10.1107/S0907444912027047>.
58. Maruyama T, et al. FT-IR analysis of BSA fouled on ultrafiltration and microfiltration membranes. *J Memb Sci*. 2001;192(1–2):201–7. [https://doi.org/10.1016/S0376-7388\(01\)00502-6](https://doi.org/10.1016/S0376-7388(01)00502-6).
59. Li Z, Qiang L, Zhong S, Wang H, Cui X. Synthesis and characterization of monodisperse magnetic Fe<sub>3</sub>O<sub>4</sub> at BSA core-shell nanoparticles. *Colloids Surf A Physicochem Eng Asp*. 2013;436:1145–51. <https://doi.org/10.1016/j.colsurfa.2013.08.044>.
60. Macdonald RD, Khajehpour M. Effects of the osmolyte TMAO (Trimethylamine-N-oxide) on aqueous hydrophobic contact-pair interactions. *Biophys Chem*. 2013;184:101–7. <https://doi.org/10.1016/j.bpc.2013.10.001>.

## Publisher's Note

Springer Nature remains neutral with regard to jurisdictional claims in published maps and institutional affiliations.